ISSN 0001-4370, Oceanology, 2006, Vol. 46, No. 5, pp. 608–628. © Pleiades Publishing, Inc., 2006.
Original Russian Text © N.A. Diansky, V.B. Zalesny, S.N. Moshonkin, A.S. Rusakov, 2006, published in Okeanologiya, 2006, Vol. 46, No. 5, pp. 650–671.

MARINE PHYSICS

High Resolution Modeling of the Monsoon Circulation in the Indian Ocean

N. A. Diansky, V. B. Zalesny, S. N. Moshonkin, and A. S. Rusakov

Institute of Numerical Mathematics, Russian Academy of Sciences, Moscow, Russia

Received August 22, 2005; in final form, March 7, 2006

Abstract—The goal of this paper is to present some results on the monsoon circulation in the Indian Ocean simulated with a σ-coordinate ocean model developed at the Institute of Numerical Mathematics, RAS. The model has a horizontal resolution of (1/8)° × (1/12)° and contains 21 σ-layers of uneven thickness. Realistic bottom topography and land geometry are used. The numerical experiments were carried out for 15 years starting from the Levitus climatology for January and monthly mean climatic atmospheric forcing from the NCEP reanalysis data. The annual cycle of the surface and subsurface currents and temperature and salinity fields were analyzed. The model reproduces well the Summer Monsoon and the Winter Monsoon currents and their time evolution and spatial structures. The Somali Current is adequately modeled. During the Summer Monsoon, the velocities of the current exceed 2 m/s, while the total mass transport is approximately 70 Sv. The model results show that a reversal of the Somali Current from the northern direction in the summer to the southern direction in the winter is accompanied by the generation of anticyclonic eddies, which drift westward owing to the β-effect and dissipate either near the Somali shore or in the Gulf of Aden. The monsoon variability of the equatorial surface current and equatorial subsurface countercurrent system are analyzed. It is shown that these currents are generated predominantly by the zonal component of wind stress, in which the half-year harmonic dominates. This leads to the fact that the equatorial surface current also changes its direction with a half-year periodicity almost in phase with the wind. The oppositely directed subsurface compensational countercurrent changes its direction with a time lag of approximately one month. Gradient currents, which appear in the Bay of Bengal due to the riverine runoff, make an important contribution to the circulation. This effect manifests itself especially strongly in the summer during the peak of the Ganges River runoff, which transports fresh turbid waters. The principal features of the large-scale quasi-stationary gyre structure of the Indian Ocean such as the Great Whirl, Socotra high, and Laccadive high and low are simulated.

DOI: 10.1134/S000143700605002X

INTRODUCTION

The Indian Ocean differs from the other oceans by a number of remarkable features. The main of them is the almost reversive changes of the powerful monsoon winds over the ocean [10, 38, 45]. As a result of this change, a strong reconstruction of the circulation in the Indian Ocean occurs during the transition from summer to winter and back. Such a change of the large-scale motions in the seasonal cycle is not observed anywhere in the World Ocean [3]. The northern part of the Indian Ocean is located in the tropics, which also determines the peculiarities of the annual evolution. These peculiarities are important for the dynamics and hydrology of the Indian Ocean.

The extremely strong seasonal (monsoon) variability and the lack of field data result in strong differences and even in contradictions between the known schemes of climatic circulation in the surface layer of the Indian Ocean (see [9, 40, 44–46, and others]). Therefore, the problem of numerical modeling of the circulation in the Indian Ocean is especially important. Different names are used in the literature for individual currents. According to different estimates, the number of the main currents with traditional names, which are manifested in the summer and winter monsoon seasons as relatively formed flows, varies from 9 to 19 [9, 44–46]. Nevertheless, the amount of data gathered in the last 20–30 years has been steadily increasing, which allowed the authors of [45] to present the most objective general schemes of the currents for the entire annual cycle.

Our paper is dedicated to the study of the Indian Ocean circulation north of 10° S, because in this region a specific monsoon circulation regime develops with reversive changes of the currents in the upper layers, which in turn redistributes heat and moisture and utilizes wind energy, being the most important regional element in the formation of the monsoon regime of atmospheric circulation [11].

In addition to monsoons, thermohaline factors also influence the circulation regime in the northern part of the Indian Ocean. The authors of [38] considered the time evolution of the highly saline water mass of the Arabian Sea and its influence on the density field and currents in the Indian Ocean. Warm and freshened waters are transported to the Indian Ocean from the

Pacific Ocean through the system of straits between Australia and Asia [28, 45]. Exchanges through these straits are important for the formation of joint meridional heat transport in the Pacific and Indian oceans at low latitudes. The authors of [19] showed that ignoring the exchange through the Indonesian straits weakens the South Equatorial and Agulhas currents of the Indian Ocean. In our model, the influence of the exchange effects through the straits is taken into account by specifying the seasonal evolution of temperature and salinity at "liquid boundaries."

MODEL OF THE CIRCULATION IN THE INDIAN OCEAN USING A σ-COORDINATE SYSTEM

In this study, we use one of the versions of the general circulation model developed at the Institute of Numerical Mathematics, RAS (INM RAS) [2]. The model is based on the primitive equations of the ocean in the Boussinesq, hydrostatic, and "rigid lid" approximations written in a spherical σcoordinate system. Horizontal components of the velocity vector, potential temperature, and salinity are prognostic variables of the model. We use the special equation of state developed for the ocean circulation models, which takes into account compressibility of water [17].

The main particular feature of this model, which distinguishes it from the well-known models of the ocean such as MOM (Modular Ocean Model) [37] in a z-coordinate system (based on the pioneer studies in [16, 20, 43]), POM (Princeton Ocean Model) [15] in a σ-coordinate system, and others (see, for example, review in [23]), lies in the fact that the splitting procedures by physical processes and spatial coordinates are used in the numerical realization of the model [5, 31].

With this goal in mind, the equations of hydrothermodynamics of the ocean are written in a special symmetrical form [5, 31]. This form makes it possible to present the operator of the differential problem as a sum of simpler operators, each of which is nonnegative, in the norm determined by the law of conservation of the total energy. Thus, it becomes possible to split the operator of the entire problem into a number of simpler operators [5, 31] and to construct spatial approximations of the corresponding groups of additives (in different equations) so that all the split discrete problems satisfy the "energetic" relation (conservation law), which is satisfied in the initial differential problem. This method in many respects eliminates the complexity of approximating the additives containing gradients of pressure, density, and bottom topography in the equations of motion written in the σ-coordinate system. The "rigid-lid" condition allows us to introduce a stream function for flat (barotropic) circulation. In this case, the method of splitting allows us to introduce the stream function only at the intermediate stage of splitting (adjustment), at which the equation for the stream function is linear [1, 31].

The method of splitting makes possible an effective realization of implicit time integration schemes for the equations of transport–diffusion of substances (the Crank–Nicholson approximation for the transport processes and an implicit approximation scheme for the diffusion and viscosity of the second order are used). The iteration block Successive Over Relaxation (SOR) method [5] is used in the integration of the equation for the stream function. The components of the Coriolis acceleration are implicitly approximated in the problem of the geostrophic adjustment. Application of implicit integration methods in time allows us to use time steps in the model, which are several times greater than in the ocean models based on explicit schemes (with similar spatial resolution). This provides a significant increase in the model computation speed, which is especially important for large integration times, for example, to gain a quasi-equilibrium state.

In order to provide a more adequate description of the ocean dynamical processes, the operator of lateral diffusion of heat and salt of the second order is presented in a form exactly equivalent to horizontal diffusion in a usual z-coordinate system [2]. The form of lateral viscosity affecting along σ surfaces usual for σ-models was conserved in the equations of motion.

The main difference of the model presented here from the version described in [2] lies in the fact that spatial differential approximations are constructed not on grid "B" but on grid "C" [35], whose dissipative property is smaller. Application of grid "C" makes possible more adequate approximation of the computation area in narrow straits, use of the slip condition at the lateral boundaries, and a decrease in the coefficient of horizontal diffusion.

The model version of the Indian Ocean presented here has a spatial resolution of (1/8)° in longitude and (1/12)° in latitude. This resolution provides a possibility to reproduce mesoscale eddy dynamics (see, for example, [22]), because it "resolves" the internal Rossby deformation scale.

Twenty-one levels by the vertical are specified. The levels are distributed nonuniformly. They are more dense in the upper layer for a better reproduction of the stratification and mixing processes in the upper layer (for example, at an ocean depth of 1000 m, the upper 100-m layer contains 9 levels).

The slip boundary condition is specified for velocity components at the lateral boundaries, while the friction condition with a linear law is specified at the bottom. Zero flux conditions are specified for the temperature T and salinity S at all the segments of the solid boundary. The bottom topography of the Indian Ocean was interpolated from the ETOPO5 dataset to the model grid and smoothed; then it was limited by a minimal value of 7 m. Nonzero depth at all the points of the domain is necessary for the σ-model's operation, because the vertical coordinate transformation is used $\sigma = z/H$ (z is the geometrical vertical coordinate, $H(\lambda, \vartheta)$ is the ocean

depth, λ and ϑ are the geographical longitude and latitude).

The model domain contains four segments of "liquid" boundaries: in the Bab-al-Mandab and Malacca straits, in the south along 10° S, and in the east along 103°5'30" E between 10° S and Sumatra Island. Temperature and salinity values from [29] are specified at the liquid boundaries from the surface to the bottom at each integration step. The account for the runoff of the main rivers influencing the salinity distribution in this version of the model is similar to the condition at liquid boundaries: the model values of salinity at each integration step are specified according to [29] over the entire depth in the regions of the mouths of the Tigris and Euphrates, Indus, Ganges and Brahmaputra, and Irrawady rivers. The model domain also contains Sri Lanka Island, at the contour of which the stream function is calculated according to the method described in [6].

In the numerical experiments, the large-scale horizontal diffusions of T and S, which parameterize the subgrid eddy activity, were taken equal to each other. The horizontal diffusion in the meridional direction A_ϑ was specified as a function of depth and latitude:

$$A_\vartheta = A\left[0.4 + 0.6\exp\left(-\frac{\sigma H}{D}\right)\right][0.5 + 0.5(\cos\vartheta)^{100}],$$

where $A = 100$ m^2/s is the maximal value of A_ϑ ($A_\vartheta = A$ at the equator at the ocean surface); and $D = 300$ m is the parameter of the exponential decay with depth. Power 100 at $\cos\vartheta$ was chosen so that the maximal value of A_ϑ is centered at the equator and smoothly decreases to half of its maximal value at 15° of latitude and remains practically the same farther to the high latitudes. The necessity of the viscosity increase in the near-equatorial region is explained by the fact that, owing to the small Coriolis force, the variability of the velocities reaches its maximal values, which increases the large-scale viscosity and diffusion.

Diffusion in the zonal direction A_λ is chosen proportional to A_ϑ as

$$A_\lambda = A_\vartheta\left(\frac{\Delta\lambda}{\Delta\vartheta}\right)\cos(\vartheta),$$

where $\Delta\lambda$ and $\Delta\vartheta$ are the steps of the spatial grid in longitude and latitude.

The coefficients of horizontal viscosity in the meridional and zonal directions were chosen similarly to those of diffusion but without decreasing with depth. In this case, the maximal viscosity in the meridional direction was equal to 1000 m^2/s.

The coefficients of vertical viscosity and diffusion were chosen according to the parameterization [36] as functions of the Richardson number Ri. The viscosity coefficient increased from 2×10^{-4} to 77×10^{-4} m^2/s, and that of diffusion increased from the background value 0.15×10^{-4} to 50.15×10^{-4} m^2/s when Ri decreased from large values to zero. In order to avoid possible outcropping of the thermocline and halocline to the ocean surface, a value of 10^{-4} m^2/s was added to the diffusion in the upper 15 m. In the case of unstable stratification, when Ri < 0, the vertical diffusion was increased up to 500×10^{-4} m^2/s, while the viscosity coefficient was chosen equal to 77×10^{-4} m^2/s (as in the case of the maximal shear instability).

CONDITIONS AT THE OCEAN SURFACE AND DESCRIPTION OF THE EXPERIMENTS

The calculation of the circulation in the Indian Ocean was performed for a period of 15 years. Wind stress was specified on the basis of the monthly NCEP reanalysis data averaged over a period from 1982 to 1994 [26]. In the first eight years, sea surface temperature (SST) and sea surface salinity (SSS) were specified on the basis of the data in [29]. During the following period, fluxes of heat and fresh water were specified at the surface, which were corrected by relaxation additions:

$$Q = Q_{sen} + Q_{lat} + Q_{lw} + 0.6Q_{sw} + c_p\rho_0\gamma_Q(T_0 - T_1),$$
$$F = P - E - \gamma_F(S_0 - S_1)/S_1,$$

where Q_{sen}, Q_{lat}, Q_{lw}, and Q_{sw} are the fluxes of sensible heat, latent heat, effective longwave and shortwave radiation; c_p and $\rho_0 = \rho(T_0S_0)$ are the specific thermal capacity and water density in the upper layer of the ocean; $P - E$ is the precipitation minus evaporation; γ_Q and γ_F are the relaxation coefficients, which have dimension of velocity; T_0 and S_0 are the SST and SSS from the data of observations; and T_1 and S_1 are the model temperature and salinity at the first level.

Similarly to the wind stress, the fluxes of heat, radiation, and fresh water are taken as monthly average values over a period of 1982–1994 from [26]; thus, they present external atmospheric forcing independent of the ocean. The coefficient 0.6 at Q_{sw} is explained by the fact that precisely this part of the shortwave radiation flux is added to the total heat flux at the ocean surface. The remaining part of Q_{sw} has a penetrating nature and exponentially decays with depth with a parameter of 20 m (see [13, 25]).

The components with γ_Q and γ_F, which take into account the observed SST and SSS, represent a negative feedback between the atmosphere and the ocean that "returns" the model temperature and salinity at the ocean surface back to the observed values of the climatic annual cycle of these characteristics. Here, T_0 and S_0 are specified on the basis of the monthly average data [29]. The coefficients $\gamma_{Q,F} = 2 \times 10^{-3}$ cm/s are chosen so that relaxation of the model T and S to the actual SST and SSS values in the upper 50 m occurs approximately during one month. The data of the NCEP reanalysis contain errors as any of the observation data (see, for example, [27]). The use of the relaxation additions to

the fluxes of heat and freshwater is one of the methods to filter out these errors and to take into account the negative feedbacks which exist in the coupled atmosphere–ocean system.

While specifying boundary conditions, all necessary monthly average input data were interpolated to the model time step using an original procedure conserving monthly average values [2].

The integration was performed from the state of rest. Three-dimensional fields for January adopted from [29] were specified as the initial data of T and S. During the 15th year of the experiment, three-dimensional fields of T, S, and velocity components (u, v, w) were output for each 5-day period. Below, these data are used to analyze the seasonal variability of the Indian Ocean circulation.

The calculations were performed using parallel program realization of the model [12] on an MBC–1000 supercomputer. The computer speed of the realization of the model written in FORTRAN 90 in the selected grid domain with a size of $524 \times 492 \times 21$ and a step of 30 min is equal to approximately 2 hours of processor time per 1 month of model time. We note that the use of the split method and special numerical schemes in our model makes it possible to perform calculations in a reasonable time with such a high spatial resolution even on personal computers.

SYSTEM OF CURRENTS IN THE INDIAN OCEAN. MONSOON CIRCULATION REGIME

The wind regime over the Indian Ocean is presented by four characteristic seasons [24, 26, 44, 45]. From May to September, the powerful and stable summer monsoon is active. Throughout this time, the direction of the winds south of the equator is southeasterly, while north of the equator their direction is southwesterly and air masses "flow" from the Southern Hemisphere to the Northern Hemisphere. From November to March, the winter monsoon is active. Throughout this time, the structure of the wind field almost mirrors the wind field of the summer monsoon. Airflow from the Northern Hemisphere to the Southern Hemisphere occurs. Monsoon asymmetry is an important peculiarity that influences water circulation, when in some regions the wind stresses of the summer monsoon exceed the wind stresses of the winter monsoon by two to four times. Typical climatic values of wind stress in January in the region of the main monsoon variability are equal to 0.5 –1.5 d/cm^2, and in July they vary from 3.0 to 4.5 d/cm^2 [24, 26].

October and April are transition months or seasons. During these transition periods, a high similarity of the spatial structure of streamlines of wind stress, which reflects the half-year cycle of the tropical atmospheric circulation in terms of climatic means, is notable. Unlike the monocentric monsoon structures, in the transition periods, three centers of different vorticity sign are manifested, namely, in the Arabian Sea, near Sri Lanka and Sumatra islands, and in the saddle near the African coast.

The half-year harmonic in the seasonal cycle of the zonal wind is formed in the equatorial region of the Indian Ocean as a result of the transition of the monsoon wind system from the summer to the winter state and back, which determines its main variability characterized by the wind direction changing to the opposite one. This determines a complex structure of the equatorial surface and subsurface currents, which also change their directions with a half-year periodicity.

According to the described regime of monsoon changes, the most intense seasonal variations in the currents occur north of 10° S, while south of 10° S the level of the seasonal signal in the dynamics significantly decreases [33, 39, 40]. Therefore, from the point of view of the monsoon variability of currents, our choice of the model region is justified. The monsoon circulation regime is most developed from the surface to depths of 20–30 m. A depth of approximately 300 m is a characteristic one, below which the monsoon signal becomes weak [9]. Thus, we shall restrict ourselves to the consideration of the main particular features of the currents in this active layer, because they are most important from the point of view of the interaction between the ocean and the atmosphere and reflect the features of the monsoon regime.

The authors of [44] presented detailed schemes of the winter and summer currents and quasi-stationary eddies, which summarize the data of ship's drifts, direct observations, calculations of Ekman's drift, and geostrophic currents, as well as satellite altimetry data. The authors of [45] demonstrate similar summarizing schemes of the currents for six months of the year (they are shown in Fig. 1). Streamlines of the mean monthly currents for odd months of the 15th year of the calculations in the 10-m surface layer of the Indian Ocean are shown in Fig. 2. The model represents well the main features of the circulation in the Indian Ocean and its seasonal variability. All the main currents determined on the basis of observations and shown in [44] and [45] (Fig. 1) are also clearly seen in Fig. 2.

Winter and Summer Monsoon Currents

The currents that were observed in January and July, which are the periods of the maximal development of the Winter and Summer Monsoon currents, are shown in Fig. 3. According to the experiments with the circulations model, the transition between the currents during the periods of the summer and winter monsoons does not occur simultaneously over the entire basin (Fig. 2). Different parts of the currents are formed at different times. A similar characteristic feature of the evolution of the currents was also distinguished from the data of observations [44, 45].

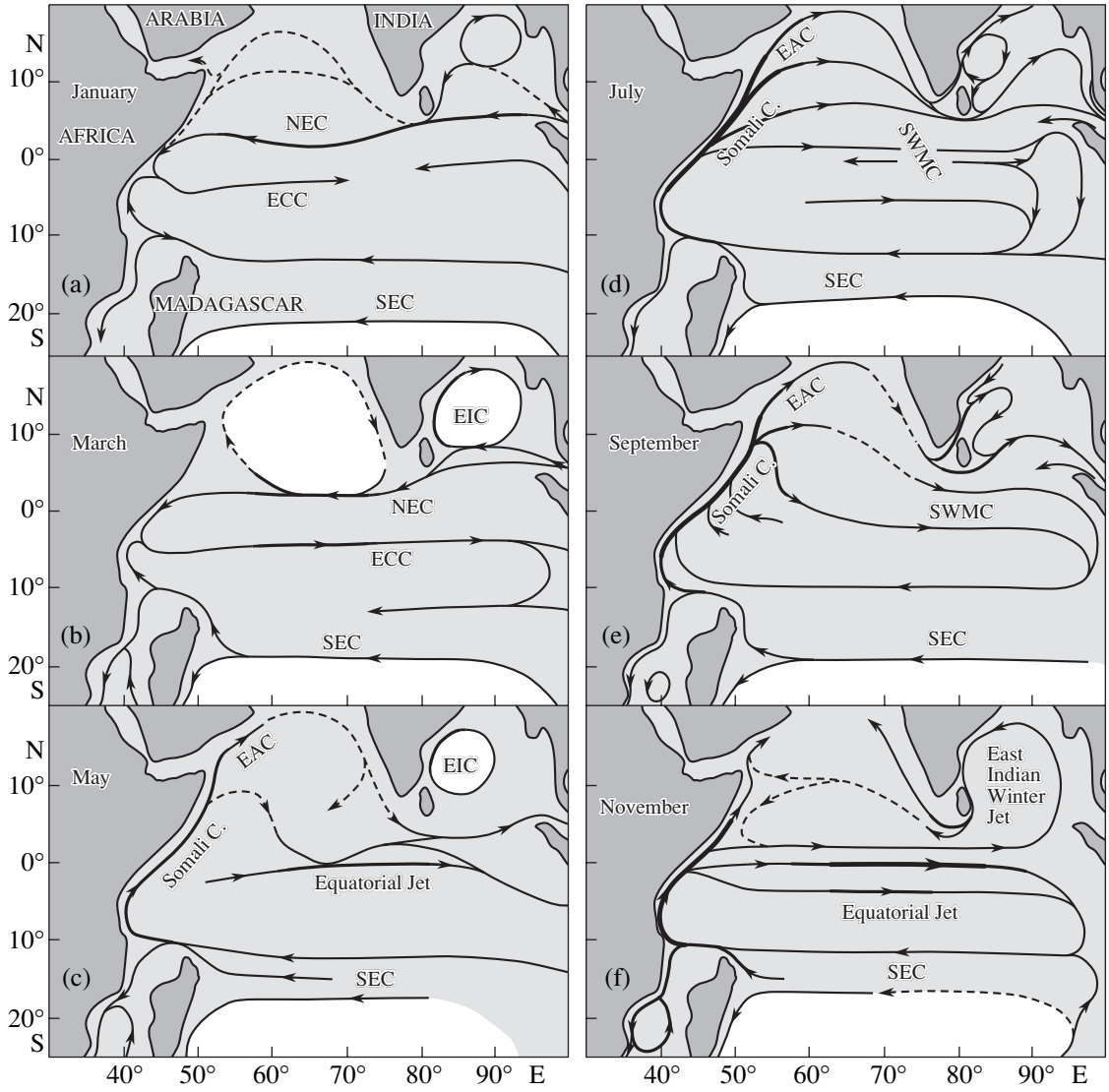

Fig. 1. Generalized schemes of the currents at the surface of the Indian Ocean based on the data adopted from [45] (abbreviations: South Equatorial Current (SEC), North Equatorial Current (NEC), Equatorial Countercurrent (ECC), Southwest Monsoon Current (SWMC), East Arabian Current (EAC), East Indian Current (EIC)).

The Winter Monsoon Current (**WMC**), according to the classification presented in [44], develops in the zone between the equator and the latitude of the southern end of India. It is directed westward of the Nicobar Islands and Sumatra up to the coast of Somali. In the region of the Maldivian and Laccadive island ridges, it branches into the northern flow directed to the Arabian Sea and its western extension. Sometimes, the WMC is called the North Equatorial Current (NEC in [9, 45]).

According to the calculations (Fig. 2), the WMC starts developing in November in the region of the southern end of the Hindustan Peninsula, which corresponds to reality [44]. In January, this current is most developed and covers the maximal area. The velocity field of the currents in the upper 10-meter layer, where the WMC is best manifested in January, is shown in detail in Fig. 3a (with the values of the velocity). It is directed to the west parallel to the Equatorial Current (see below) forming a joint flow with it, which covers the entire ocean north of 2° S. According to the calculations, the eastern part of the WMC consists of two branches. The northern branch flows from the Andaman Islands to India and Sri Lanka Island originating from the Strait of Malacca. The southern or main branch is a continuation of the Equatorial Current (EC) originating from the Sunda Strait between Java and Sumatra. We shall use the term EC understanding that, according to [44], the surface current at the equator is directed westward if not specially noted. In the upper layer, which is 10–20 m thick, the velocities in the WMC reach their maximal values of 70–100 cm/s at the longitude of the southern extreme end of India and southwest of this

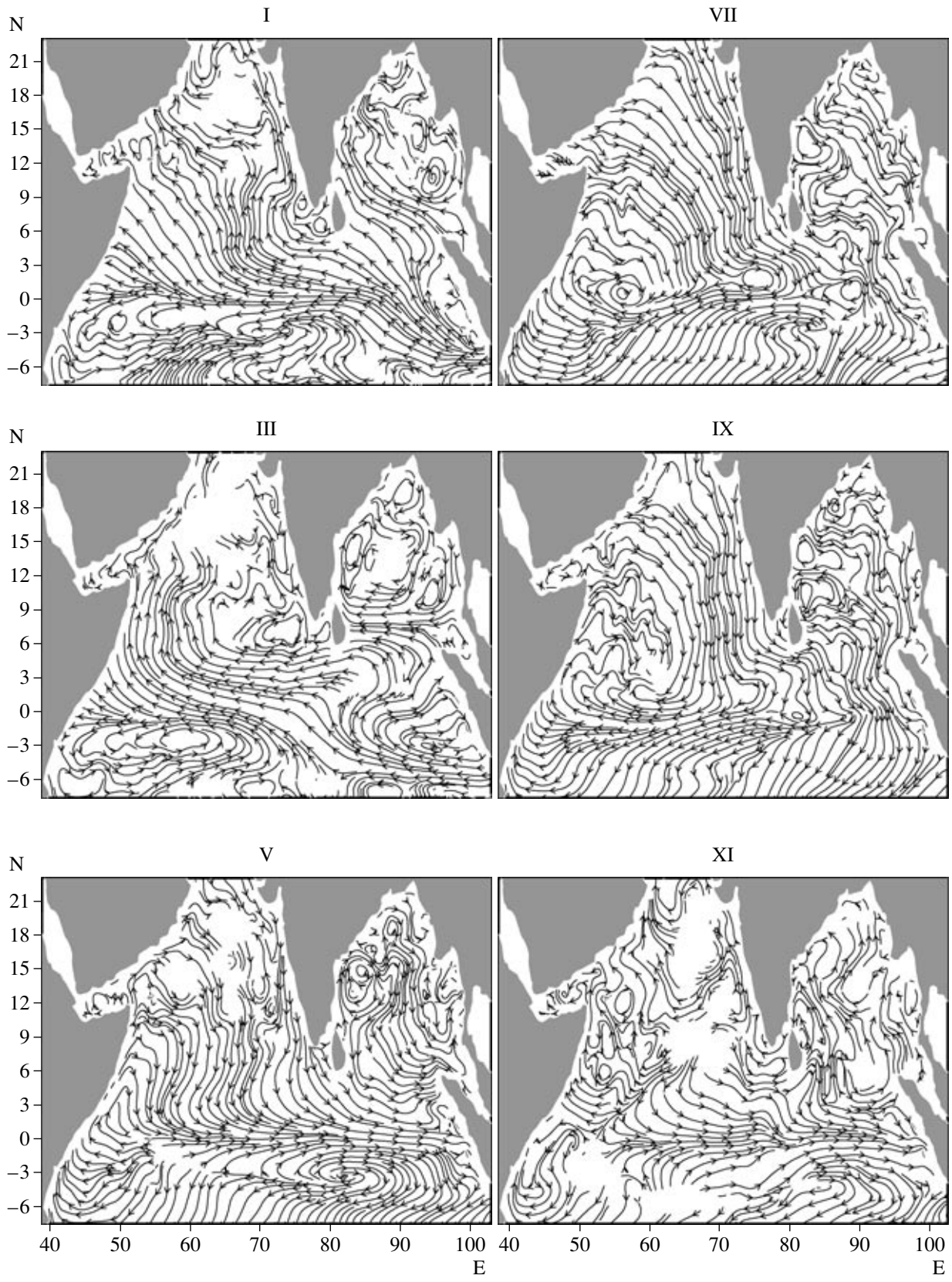

Fig. 2. Streamlines of the mean monthly currents for 6 months with odd numbers of one year in the surface 10-m layer of the Indian Ocean. Velocities less than 5 cm/s are not shown.

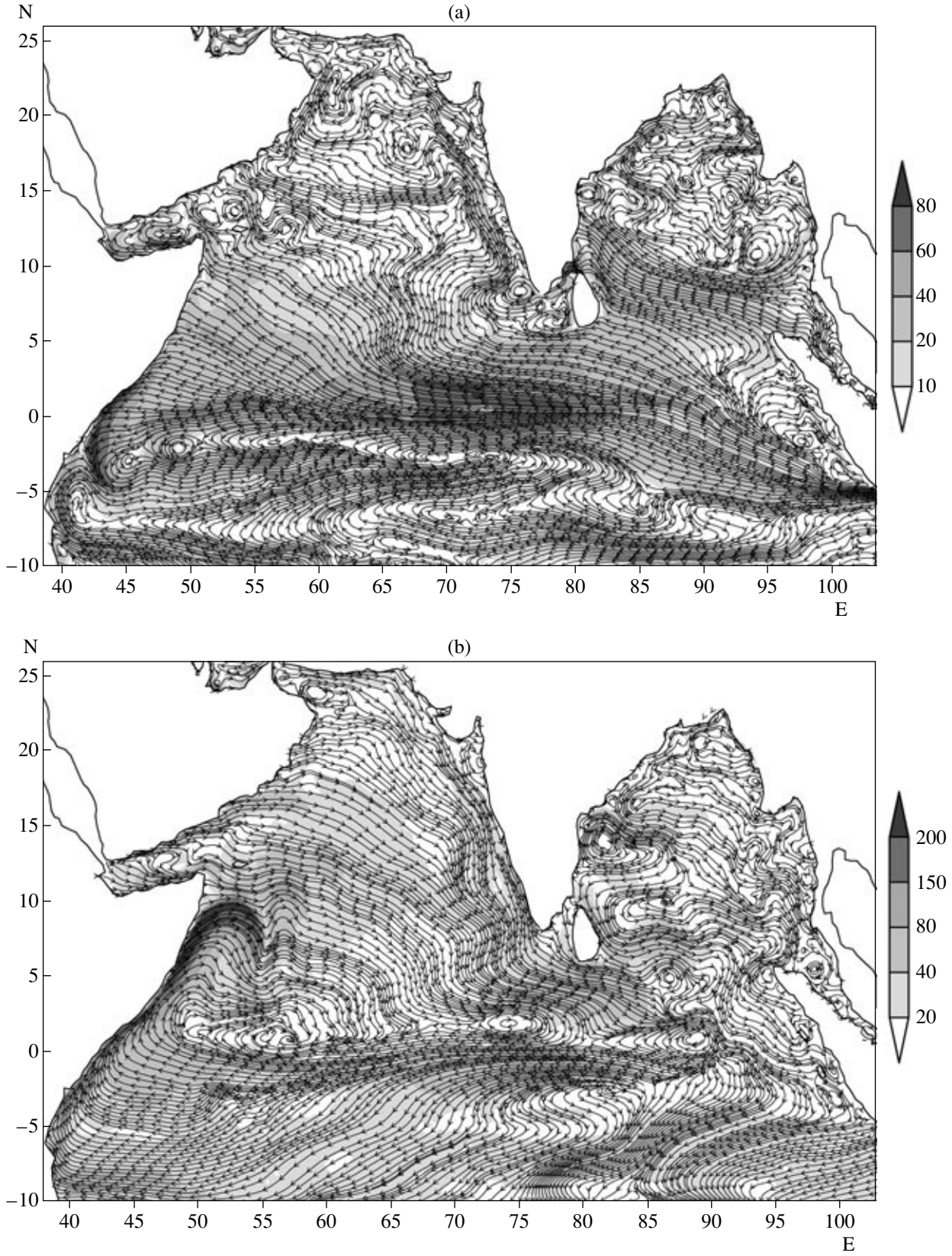

Fig. 3. Mean currents for (a) January and (b) July in the surface 10-m layer of the Indian Ocean. The streamlines of the currents are shown. The velocities (cm/s) are shown with gradations of gray color. The color scale is shown on the right.

point (60°–80° E, Fig. 3a). Here, a sufficient wind fetch is gained, while the separation of the WMC into the Arabian and western branches has not yet started. The western branch of the WMC as a spatially uniform flow reaches the African coast, masking a complex structure of the coastal currents located deeper than 30–40 m.

Two flows separate from the western part of the WMC to the north into the Arabian Sea in the region of the Maldive and Laccadive islands (the Chagos–Laccadive Ridge) and west of this region near the Arabian–Indian (Carlsberg) Ridge, which correlates with the data of observations [44]. The first flow is the Western Indian Coastal Current (WICC) (see Figs. 1 and 3a), in which the velocities in the upper layer reach 50 cm/s and more. The second flow covers a much greater area with velocities in the upper layer not exceeding 20–25 cm/s directed to the Arabian coast.

The Summer Monsoon Current (**SMC**) is directed to the east across the entire ocean from Africa and Arabia to Sumatra (the Summer Monsoon Current is adopted from [44] and Southwest Monsoon Current (SWMC) is adopted from [45]; see SWMC in Fig. 1). Owing to the reverses in the wind system, it reversibly replaces the WMC.

According to our calculations (Fig. 3b) and to the data of summarized observations [44], the SMC has two "sources" in the western part of the Indian Ocean. In the southwest of the Arabian Sea, it is supplied by the waters of the Somali Current not involved into the Great Whirl. The second source of the SMC is the alongshore WICC, which, in turn, is formed by the drift currents of the Arabian Sea over the shelf of Hindustan. The velocities of the SMC forced by the wind south of the Hindustan Peninsula reach their maximum (up to 80–150 cm/s according to our estimates) south of Sri Lanka Island (Fig. 3b).

The southern boundary of the SMC is the convergence line between the SMC and EC, which, according to our calculations, consists of a series of anticyclonic eddies 100-200 km in size stretching over the entire ocean from Somali up to 96° E (see Fig. 3b). The SMC splits into two branches over a submarine rise at coordinates 5° N, 85° E and depth differences of approximately 1.5 km (Fig. 3b). The northern branch accumulates the current of the southern direction off the eastern coast of Sri Lanka, enters the Bay of Bengal as a wide flow, reaches the Nicobar Islands, turns to the south and southeast near the coast (this turn starts at 92° E), and merges with the southern branch of the SMC. The SMC crosses the equator along the southern shelf of Sumatra and merges with the South Equatorial Current (Fig. 3b).

Somali Current

The next characteristic element of the reversive wind-driven monsoon circulation is the Somali Current (see Figs. 1–4), which is "a calling card" of the Indian Ocean like the Winter and Summer Monsoon currents considered above [42].

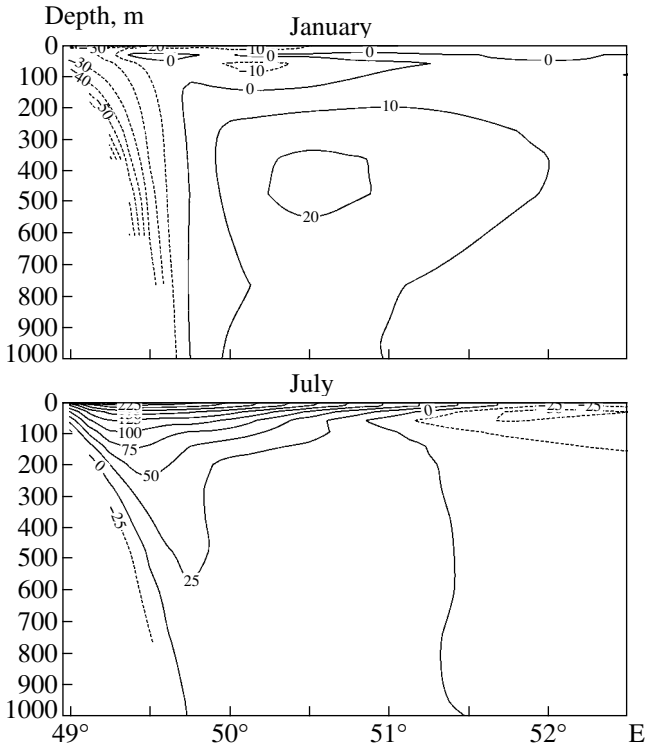

Fig. 4. Alongshore velocity in the Somali Current (SC) in cm/s averaged (above) over January and (below) over July. Section along 6° N near Somali coast in the layer 0–300 m. The positive values correspond to the northeastern direction; the negative values refer to the southwestern direction.

The Somali Current (SC) ([44, 45]) is a alongshore reversive western boundary jet current. During the summer monsoon it is directed to the northeast, and during the winter monsoon it flows to the southwest. An analysis of the results of numerical experiments confirmed that the SC is caused by direct wind forcing (local maxima of wind stress during the summer and winter monsoons) and by the large-scale compensating mechanism of mass flux near the coastal barrier in the near-equatorial region of the ocean during the monsoon (seasonal) cycle of circulation evolution (see also [32, 41]) (the jet closing the system of near-equatorial and monsoon currents in the entire ocean).

In the summer, the SC is so intense and powerful that in some publications the SC is interpreted as a current that exists only in the period of the summer monsoon from May to September [45]. In the summer, its velocities in the upper layer of the ocean reach 100 cm/s according to the data in [9], and 200–250 cm/s according to the data in [41]. Our calculations correspond to the latter of these estimates. The horizontal structure of the SC is clearly seen in Fig. 3, which reflects the results of the numerical experiments.

In the summer (July), in the zone 300–350 km wide near the coast between 2°–3° S and 10°–11° N, the SC is represented by a jet with velocities up to 200 cm/s or more. During this period, the SC is supplied by the waters from the near-equatorial system of currents in the zone between 10° S and 2° N and transports its waters to the SMC (Fig. 3). In July, according to our estimates, the maximal transport of the Somali Current can exceed 70 Sv. The authors of [9] give an estimate of 54 Sv obtained on the basis of a dynamical method of calculations. According to our calculations, this estimate, which relates to the maximal transport of the SC, should be considered as an underestimation, because it was calculated from the smoothed data of a one-degree density field and does not take into account the drift component of velocity.

The distribution of the alongshore velocity of the Somali Current over a section along 6° N in July and January in the upper 300 m is shown in Fig. 4. The velocity field is reproduced adequately to the known data (see [41, 45, and others]). In the summer (July), the core of the current with velocities exceeding 100 cm/s is located in the layer between the surface and 90–100 m (the velocity in the upper 20 m is 200–250 cm/s). In January, velocities do not exceed 65 cm/s. In the summer, the core of the SC is located at the ocean surface at a distance from the coast, and in the winter it is located deeper than 200 m and is "displaced" to the coast. It is clearly related to the influence of the Coriolis force, which in the summer displaces the current jet from the coast, and in the winter, on the contrary, displaces it toward the coast. In the summer, these processes are accompanied by the formation of a powerful coastal upwelling, which transports slowly moving deep waters upwards, and in the winter they are accompanied by a downwelling, which transports the momentum of the SC down from the surface.

In the summer, the extremely intense coastal upwelling in the SC is clearly marked by the waters with a decreased temperature [9, 32, and many others]. A comparison of the model and experimental temperature distributions according to the present-day general climatic conclusions based on the data of observations with a resolution of 0.25° [18] showed an adequate reproduction of the upwelling both in the Somali and West Arabian (Oman) coastal currents. In the region of the most intense upwelling, the temperature decreases to 20°C and even lower, while in the open ocean at the same latitudes the temperature is 27–28°C. The horizontal sizes and configuration of the region, in which the temperatures in the upper layer are below 25°C, are identical according to the model and data of observations. The upwelling in the SC manifests itself only from 3° N, reaching a maximum at 8°–10° N near the coast of the Somali Peninsula. This is explained by the fact that the influence of the Coriolis force near the equator is insignificant and generates no displacing effect, needed for an upwelling, in the near-equatorial zone near the coast.

The analysis of the time evolution of the SC on the basis of the 5-day data of calculated fields of currents showed a very interesting physical feature. The change in the direction of the current field from summer to winter is accompanied by the generation of anticyclonic eddies, which are displaced to the west under the influence of the β-effect and dissipate near the African coast. A small part of them penetrate to the Gulf of Aden and generate an eddy field there, which is not correlated with the local atmospheric conditions and exists autonomously during a certain period in the winter.

East African Coastal Current

The authors of [44] distinguish the East African Coastal current. It is directed to the north along the African coast from 10° S to 2° S and does not change its direction throughout the whole year.

The East African Coastal Current (EACC) [44] is a link between the South Equatorial Current and Equatorial Countercurrent, providing the mass balance in the upper layer and closing the southern cell of near-equatorial circulation in the Indian Ocean.

The EACC is clearly reproduced in the numerical experiment (see Fig. 3). In winter, it is clearly manifested, forming a convergence zone with the Somali Current near the African coast at 2°–4° S. In summer, it is collinear with the Somali Current and looks like a source of the SC (see Fig. 3b). According to the calculations of velocity in the EACC, they reach 50 cm/s in winter of the Northern Hemisphere and increase in summer to 100 cm/s. This evolution of the EACC reflects a global intensification of the circulation system in the upper layer of the Indian Ocean from winter to summer.

System of Equatorial Currents

Variability in the system of equatorial currents of the Indian Ocean is characterized by a clearly manifested half-year period caused by the similar period in the wind stress. Annual evolution of the mean zonal velocity of the currents in the layers 0–20 m and 110–220 m and zonal wind stress at the equator at 73° E are shown in Fig. 5. The authors of [34] present the results of long-term regular observations of zonal velocity of currents at the equator at 73° E for 1973–1975 in the layer 0–20 m. A comparison of the data of calculations and observations demonstrated their coincidence both in phase (half-year cycle) and amplitude (approximately 100 cm/s).

Let us consider the currents in the open part of the near-equatorial zone of the Indian Ocean (not including the basins near the coasts of Sumatra east of 90° E and Africa), which are characterized by regional peculiarities. In order to get a concept of the spatiotemporal structure of equatorial currents, let us divide their time evolution into 8 types according to Fig. 5: (**1**) January 10–February 20; (**2**) March 10–March 31; (**3**) May 01–May 31;

(**4**) June 10–June 30; (**5**) July 10–August 25; (**6**) September 15–October 15; (**7**) November 01–November 30; and (**8**) December 10–December 31. Four of them correspond to the extremes of the velocities of the surface currents, the other four to their transition regimes. During transition periods, subsurface currents in turn obtain extreme values; i.e., a phase shift of approximately one month is observed between the extreme values of the velocities in the surface layer (phase advance) and in the subsurface layers (phase lag). Since we demonstrate mean patterns of the currents, their values are 20%–30% smaller than the peak ones.

(**1**) In January–February, a special type of near-equatorial circulation is formed (see Figs. 6 (1), and Fig. 3a). During this period, a westward current exists near the equator from 2° S to 6°–7° N in the layer from the surface down to 50–80 m with velocities at the surface of 70–100 cm/s, which is a joint flow of the EC and WMC. The authors of [45] distinguish this flow as the North Equatorial Current (abbreviation NEC in Fig. 1). In the winter, this flow (EC plus WMC) is the main element of the westward transport. It is most developed in February, while in March its velocities decrease on the average to 20–25 cm/s (Fig. 6 (*2*)). It contains two cores: at the equator and at 1.5°–2.0° N. The authors of [44] distinguish this flow as two independent flows. In the winter, the South Equatorial Current (SEC) located south of 7° S also transports water to the west but to a lesser degree (Fig. 6: (1), (2), and (8)).

During the three winter months, the Equatorial Countercurrent is clearly manifested between the EC and SEC in the zone from 2°–2.5° S to 6° S. This current is directed to the east, i.e., oppositely to the currents surrounding it. According to the generalized data of observations, it is determined either as the South Equatorial Countercurrent [44] or as the Equatorial Countercurrent (ECC in Fig. 1). In January–February, the 10 cm/s isotach of this current reaches a depth of 80 m (Fig. 6(1)).

In January–February (Fig. 6 (1)), in the 2–3 degree equator zone, the Subsurface Equatorial Countercurrent of the eastern direction (SECCED) begins to form at depths greater than 50 m, which was experimentally discovered by Soviet oceanographers in 1960 and was named the Tareev Current [4].

(**2**) In March, a drastic reconstruction of the equatorial current system occurs, which is related to the alteration in the wind direction (Fig. 5). During this period, the Tareev Current reaches its maximal development in the layer from 40 to 350 m (Fig. 6 (2)). The core of the current is located at depths of 80–150 m and its velocities exceed 25 cm/s, reaching 30–40 cm/s in selected regions. This current is a characteristic element of the transition circulation, which is best manifested in March and in September–October (Fig. 6: (2) and (6)). The Tareev Current is located under the EC and directed to the east oppositely to the EC. Together with the ECC, it transports water to the east (Fig. 6).

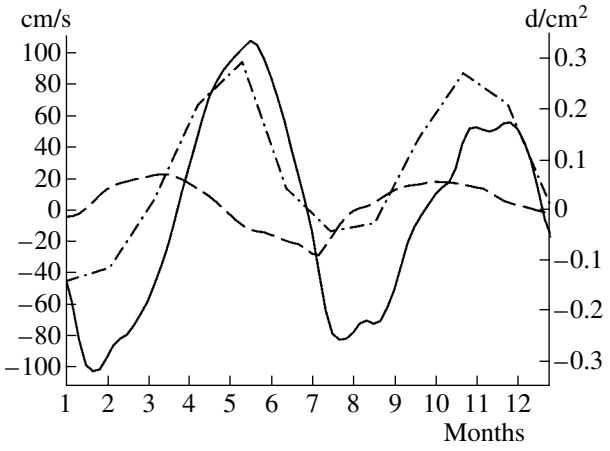

Fig. 5. Annual evolution of the current velocity and zonal wind stress. The average velocity in the layer 0–20 m is shown with the solid line and that in the layer 110–220 m is shown with the dashed line. The wind stress at the equator at 73° E is shown with the dashed–dotted line. The velocity scale in cm/s is shown on the left. The wind stress scale in d/cm^2 is shown on the right. The positive values correspond to the eastern direction; the negative values refer to the western direction.

The current near the equator changes its direction from the west to the east and, in April, finally stabilizes along the direction of the wind (in April, westerly winds dominate at the equator). In March, the mean monthly velocities in the EC reached 50 cm/s and more, while at the end of April the velocities of the already eastward current also reach 50 cm/s. At the same time, at the beginning of April, all other elements of the monsoon circulation remain almost identical to the winter ones. In April, the Tareev Current is collinear with the eastward EC. They form a single eastward flow with two cores with respect to the vertical from the surface to 200 m almost symmetrically with respect to the equator in the 2–3 degree neighborhood of the equator. The core of the WMC is displaced to the north to 5° N and the velocities in the WMC are reduced. At the end of April, in the zone 0°–2° N, a compensation westward flow with respect to the eastward EC starts to form deeper than 300 m.

(**3**) From May to June, the SMC begins to develop. It merges with the Equatorial Current of the eastern direction and occupies the upper 100–150 meters (Fig. 6 (3)), forming a single powerful flow with velocities at the surface up to 90–100 cm/s or more in the zone from 2°–3° S to 5° N. This reconstruction is clearly distinguished on the basis of the data of observations, and the new term "Equatorial Jet" was even introduced for this flow [45] (see Fig. 1). We shall call it the Equatorial Current of the Eastern Direction (ECED). During this period, south of 2°–3° S in the layer from the surface to 30–50 m, a westward compensating transport appears that can be identified with the SEC, which in other seasons begins only south of 5°–7° S. In June, the

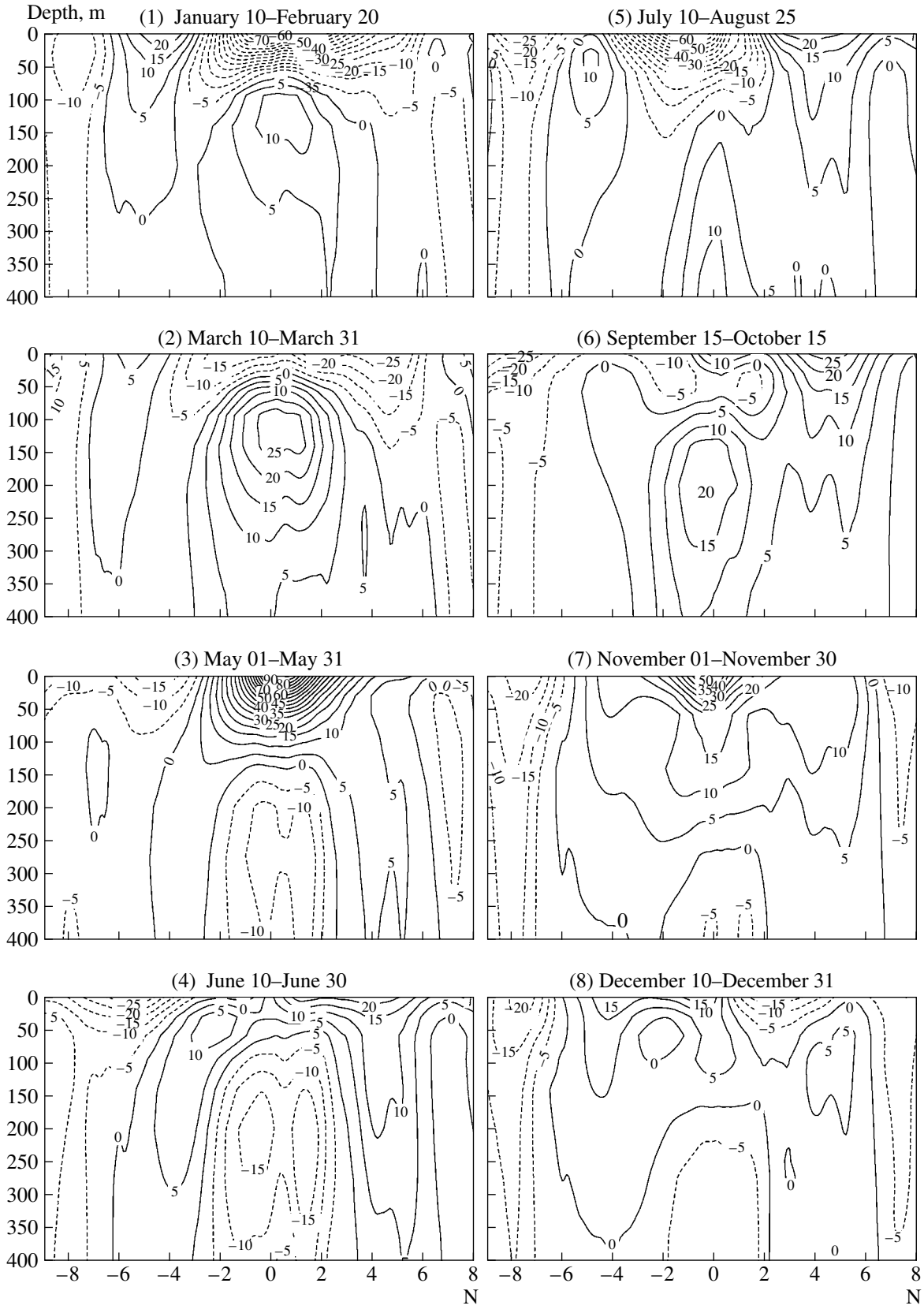

Fig. 6. Meridional sections of the vertical structure of the zonal velocity near the equator from 9° S to 8° N. Zonal averaging was performed from 65° E to 80° E. Time averaging was performed over periods shown for each section. The solid lines denote isotachs of the eastern direction; the dashed lines denote isotachs of the western direction (in cm/s).

velocities at the surface in the SEC reach 30–40 cm/s (Fig. 6: (3) and (4)).

In May, the compensation subsurface flow, which began at the end of April, becomes clearly manifested as a westward current with two cores located horizontally almost symmetrically in a 2-degree neighborhood at the equator in the layer 150–500 m, where mean velocities exceed 10 cm/s (Fig. 6 (3)). This current can be identified as the Subsurface Equatorial Countercurrent of the Western Direction (SECCWD).

(**4**) In June, a new reconstruction of the structure of equatorial currents starts. The ECED weakens and splits into the southern and northern branches (Fig. 6 (4)). In this case, the southern branch can be identified with the newly formed ECC, which starts forming during this period, while the northern branch can be identified with the SMC. During the transition period from June to July, the EC is formed again owing to the change of the wind. In June, the SECCWD penetrates to a maximum depth over the year reaching 500 m. In this period, the current reaches the maximum of its development, when mean velocities exceed 15 cm/s (Fig. 6 (4)), while at 73° E (Fig. 5) these velocities reach 40 cm/s, becoming as large as the velocities of the Tareev Current in March. At that period of time, the SECCWD is presented by two velocity peaks (cores) near the equator located in the layer 50–500 m (Fig. 6(4)).

(**5**) In July–August, the summer monsoon regime of the atmospheric circulation is established, and the next type of equatorial current is formed. In that period, the EC intensifies and absorbs the ascended SECCWD. Mean velocities in the EC exceed 50 cm/s (Fig. 6 (5)). The core of the EC is located at 1°–2° S on the average, where in August velocities reach maximal values of 100 cm/s or more in a number of regions. In that period, south of 2° N, the flows of the EC and SEC form a westward transport in the upper layer. The core of the SEC displaces to 5°–6° S (Fig. 6 (5)). The EC and SEC are separated by the oppositely directed eastward ECC (Fig. 6 (5)). Unlike other seasons, in July–September (up to the beginning of October), the ECC exists as a flow of water under the ocean surface. In July–August, the center of this current is located in the layer 30–200 m in the region of 3°–4° S and it outcrops to the surface only in some regions. Thus, on the average, over the area of the EC and SEC, they form a joint westward flow at the ocean surface south of 2° N. In August–September, the center of the ECC ascends to the layer 20–60 m and is displaced to 5°–6° S; the upper boundary of the ECC reaches the surface (Fig. 6 (5)). In July, the eastward SMC continues intense development north of 2°. It consists of the surface and deep (at 100–250 m) jets. Both are located at 3°–4° N (see location of the isotachs 5–10 cm/s in Fig. 6(5)).

The major part of the regularities of the circulation found in the numerical experiment during this period is also reflected in the schemes of the summarized data on the surface currents of the Indian Ocean in July and September published in [44, 45]. Some elements of the circulation were studied in more detail in the calculations. As an example, we note that, in the scheme of currents in September published in [45], it was shown that the SMC includes the region of the equator. According to our data, the convergence line separating the SMC and EC is located at the surface at 2° N during the whole summer including September, and the current at the equator west of 80° E is directed to the west (Figs. 2b, 6 (5)).

At the end of August, the SECCED (Tareev Current) starts to form again, ascending from depths on the order of 500 m with velocities in the core exceeding 10 cm/s (Fig. 6 (5)). In the middle of September–beginning of October, the SECCED reaches its maximal development (autumnal maximum) at the equator at depths from 100 to 400 m. Its eastward velocities opposite to the EC exceed 20 cm/s in the layer 150–250 m. However, it is less intense than in the period of the winter phase (compare Figs. 6: (2) and (6)).

At the end of August and the beginning of September, the SMC and SEC are practically unchanged. In November, the EC begins to decay and yields to the intense ECED. Throughout this time, the ECC weakens and almost disappears.

(**7**) In October–November, the ECED "absorbs" the weak SMC and ECC, sets in, and during the period from the end of October to December reaches its maximal development with velocities of 60–70 cm/s at the ocean surface near the equator in November (see Fig. 6 (7)). During the period from the end of October to November, the following events occur: (a) the SECCED ascends to the surface and merges with the ECED; (b) the South Equatorial Current (SEC) intensifies; and (c) north of 6° N, a westward jet begins to form, which further transforms to the WMC. Thus, in the autumn, the eastern water transport absolutely dominates, while the currents (SEC) of the western direction south of 2°–6° S are weak (see Figs. 6 (6) and (7)).

(**8**) In December, the system of near-equatorial currents passes a strong reconstruction: the eastern mass transport at the equator changes to the western (compare Figs. 6 (8) and (1)). North of the equator, the formation of the EC begins, whose core in that period is located near 2° N. The ECED decays and weakens, leaving fragmentary formations (Fig. 6 (8)), the main of which is the ECC. The SEC is almost unchanged, while the WMC slightly intensifies.

The results of the analysis of the near-equatorial circulation in the Indian Ocean are presented in the table.

Subsurface Equatorial Countercurrents

Because of the historical reasons of the observations, the Tareev Current is understood as a subsurface eastward flow in the winter period opposite to the Equatorial Current [9]. The Tareev Current develops in the

Characteristics of the near-equatorial circulation in the Indian Ocean

No.	Period	Eastward transport	Westward transport
1	January–February	ECC and SECCED	WMC, EC, and SEC
2	March	ECC and SECCED	WMC, EC, and SEC
3	May	ECED and SMC	SECCWD and SEC
4	June	SMC, ECED, and ECC	SECCWD and SEC
5	July–August	SMC and ECC	EC and SEC
6	September–October	SMC, SECCED, and ECED	SEC
7	November	ECED	SEC
8	December	ECED and ECC	WMC, SEC, and SECCWD

Note: SMC and WMC are the Summer and Winter Monsoon currents; EC, ECC, and ECED are the Equatorial Current, Equatorial Counter Current, and Equatorial Current of the Eastern Direction; SEC is the South Equatorial Current; SECCED (Tareev Current) and SECCWD are the Subsurface Equatorial Countercurrents of the Eastern and Western directions.

2–3 degree zone around the equator. It is an analogue of the Cromwell and Lomonosov currents in the Pacific and Atlantic oceans [9, 14]. Our experiments demonstrate the existence of the Subsurface Equatorial Countercurrent (SECC) almost throughout the entire year (Fig. 6). Its flows of the eastern (SECCED) and western (SECCWD) directions are distinguished. The nature of this current is compensatory with respect to the equatorial currents at the surface. This is confirmed by the fact that the intensity of the SECC correlates with the surface equatorial flow, while the extreme values appear with a time lag of approximately one month as compared to the equatorial flow at the surface. Since a significant inertia is typical for the SECC, it is collinear with the EC or ECED during the transition periods of the wind field and ocean circulation reconstruction, i.e., it loses the properties of a countercurrent.

Intensification of the SECC is correlated with the ascent of its core to the ocean surface. The maximal near-surface development of the SECC characteristic of its eastern phase of direction (SECCED or Tareev Current) takes place in February–March and in September–November. The Tareev Current reaches its maximal development in March, when it is actually a countercurrent with respect to the Equatorial Current. In selected regions, its velocities reach 40 cm/s or more. In the autumn, the velocities of the SECCED are maximal in October. The stages of the surface and, correspondingly, maximal development of the SECCWD take place in May–July and in December (secondary maximum). On the average, the velocities reach 30 cm/s in the core of the SECCED and 20 cm/s in the core of the SECCWN.

The meridional vertical (transversal) structure of the SECCWD is characterized by two cores north and south of the equator (see Figs. 6: (3), (4), and (7)), whereas the SECCED is always represented by a single core. This is caused by the fact that the current of the western direction near the equator is subjected to the influence of the Coriolis force directed to the north and south from the equator, which causes "splitting" of the flow into the northern and southern parts. In contrast, currents of the eastern direction are drawn together to the equator. Owing to this cause, the velocities in the SECCED should be greater and more stable than the velocities in the SECCWD, which is confirmed by our calculations. The same can be said about the ECED and EC at the surface (compare the characteristic states in Figs. 6: (2) and (3)).

Figure 7 gives a possibility to compare the Tareev Current and SECCWD in the periods of their maximal development. Vertical sections of the currents averaged over the last ten-day periods of February and May, respectively, in the zone between 1.5° S and 1.5° N along the equator in the layer 0–400 m are shown in this figure. The Tareev Current has a homogeneous structure with a core at 75–175 m along the entire Indian Ocean. In the region 60°–85° E, mean velocities reach 30 cm/s with the maximal values at 49° E and 80° E reaching 40 cm/s or more. During its maximal development, the SECCWD, unlike the Tareev Current, is spatially inhomogeneous and divides into two parts near the Maldivian Ridge (73° E). Its eastern part is more intense, with velocities up to 30 cm/s and a smaller depth of the core (150–300 m) as compared to the western part. The velocities in the western part are signifi-

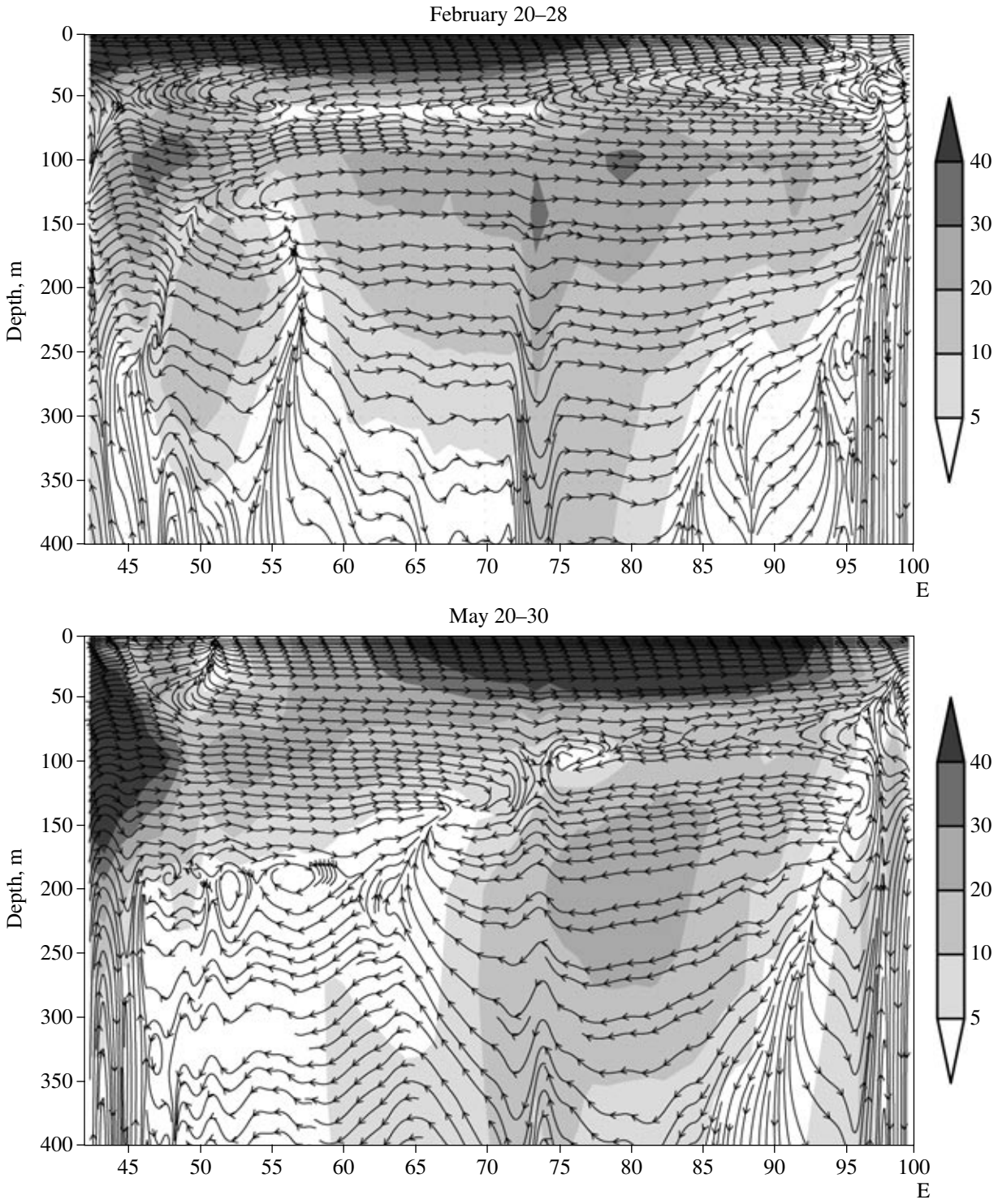

Fig. 7. Vertical sections of the currents (stream lines) along the equator in the layer 0–400 m averaged in the zone between 1.5° S–1.5° N: (above) the last ten days of February; (below) the last ten days of May. The velocities in cm/s are shown with gradations of gray (color scale is shown on the right). For illustrative purposes, the vertical component is multiplied by 10^3.

cantly smaller (down to 10 cm/s), and the core is located deeper than 250 m.

Summarizing the analysis performed, we note the following:

(1) The SECC has a compensating nature with respect to the flow of the EC or ECED of the wind origin at the surface. It is located strictly at the equator under the sea surface in the 2–3 degree neighborhood of

the equator. Its orientation in the periods of maximal development is always opposite to the surface current at the equator.

(2) The increase in the velocity of the SECC to the maximal values occurs with a time lag of approximately one month after the formation of the surface EC or ECED. The process of formation and intensification of the SECC looks like its ascent from depths greater than 400 m. The more intense the surface current at the equator, the more intense the SECC.

(3) When the direction of the surface current at the equator changes, the SECC exists due to inertia and loses the properties of a countercurrent. Thus, during this period, both flows are collinear (April is the best example). Later, the SECC is "absorbed" by the surface current, and after this the SECC is formed again as a countercurrent but of the opposite sign. According to the half-year cycle of the near-equatorial circulation, such reconstruction of the currents is observed four times a year.

(4) A change of monsoons (monsoon cycle of the near-equatorial circulation) generates phases of the SECC of the eastern (SECCED) and western (SECCWD) direction. The half-year cycle of the near-equatorial circulation determines two periods of each of the phases: eastern and western. The SECCED is observed in February–March and in October–November, while the SECCWD is observed in June–July and in December.

(5) Since the current of the western direction near the equator is subjected to the influence of the Coriolis force directed to the north and south from the equator, a transversal separation of the flow into the northern and southern parts occurs. In contrast, the Coriolis force at the equator concentrates the current of the eastern direction; therefore, its velocity and stability are greater. Thus, during the phase of the eastern direction, the velocities in the SECC are one and a half to two times greater than during the western phase, and the core of the flow is located significantly closer to the ocean surface. The total duration of the SECCED phase is approximately two times as great as that of the SECCED phase.

(6) The SECCED is represented by a relatively homogeneous long flow along the equator at depths 75–175 m, whereas the SECCWD is divided into two parts by the Maldivian Ridge. West of the ridge, it deepens by approximately 100 m with respect to its eastern part located at depths of 150–300 m.

Currents in the Bay of Bengal

The main circulation element in the Bay is the East Indian Coastal Current (EICC) according to [44], or the East Indian Current according to [45], or the West Bengal current according to [9]. According to [44], the EICC occupies the entire eastern coast of India. It is distinguished by a characteristic reversive change of directions typical of the monsoon regime. In the winter, it is directed to the southwest from the mouth of the Ganges to Sri Lanka Island, i.e., the general cyclonic circulation regime is realized. In the summer, it is oppositely directed to the northeast and the anticyclonic regime is realized.

Besides the EICC, the authors of [9] distinguish the East Bengal Current, which is also an alongshore flow with a mean velocity of 15 cm/s. Together with the EICC, it forms an anticyclonic gyre of the Bay of Bengal. The authors emphasize that this gyre is practically not subjected to the seasonal (monsoon) variability (only the exchange with the ocean in the southern part of the bay changes related to the change between the Summer and Winter Monsoon currents). Thus, the EICC is directed to the northeast throughout the entire year. They present the parameters of the EICC: the width is 200–250 km, the velocity at the surface in the summer is 25 cm/s and 17 cm/s in the winter; the depth of penetration in the summer is 300 m and 100 m in the winter. In the numerical experiment, the EICC is more intense in the winter and its width is close to 200 km, while the velocities reach 30–40 cm/s, which notably distinguishes the EICC against the background of the rather slow anticyclonic motion of the waters in that region.

According to [45], in the summer (July), the northeastward EICC is related to the existence of a stable anticyclonic gyre with a size of approximately 400–500 km (near the western coast of the bay). This is the most principal difference of this scheme of the currents from the other ones (see Fig. 1). In the winter (January), a weak anticyclonic rotation of waters is found in the center of the bay with a diameter of 800–1000 km, while the alongshore currents poorly manifest themselves. The anticyclonic circulation regime is realized only in the late autumn (Fig. 1). Thus, significant differences are found between the circulation schemes of the upper layer in the Bay of Bengal published in [9, 44, 45].

According to the results of the numerical experiment, drift currents are developed in the southern part of the bay south of 12°N, which are the northern periphery of the Winter and Summer Monsoon currents with a prevalence of the pure drift Ekman transport (velocities in the winter are 30–40 cm/s, and in the summer they are up to 50–70 cm/s) (see Figs. 2, 3a, and 3b). This result correlates well with publications [44] and [45]. In the summer (July), the intense anticyclonic rotation of the waters is well reproduced in the region between 12° and 16° N near the western coast of the bay (Figs. 2, 3b). Thus, the numerical experiment confirms precisely the scheme in [45]. The size of the anticyclonic formation over the meridian is 400 km and 600 km in latitude. This is "related" to the turn in the coastline of India by 45° (near the mouth of the Krishna River). The maximal velocities in the bay (up to 60–80 cm/s) are related to the northern periphery of this

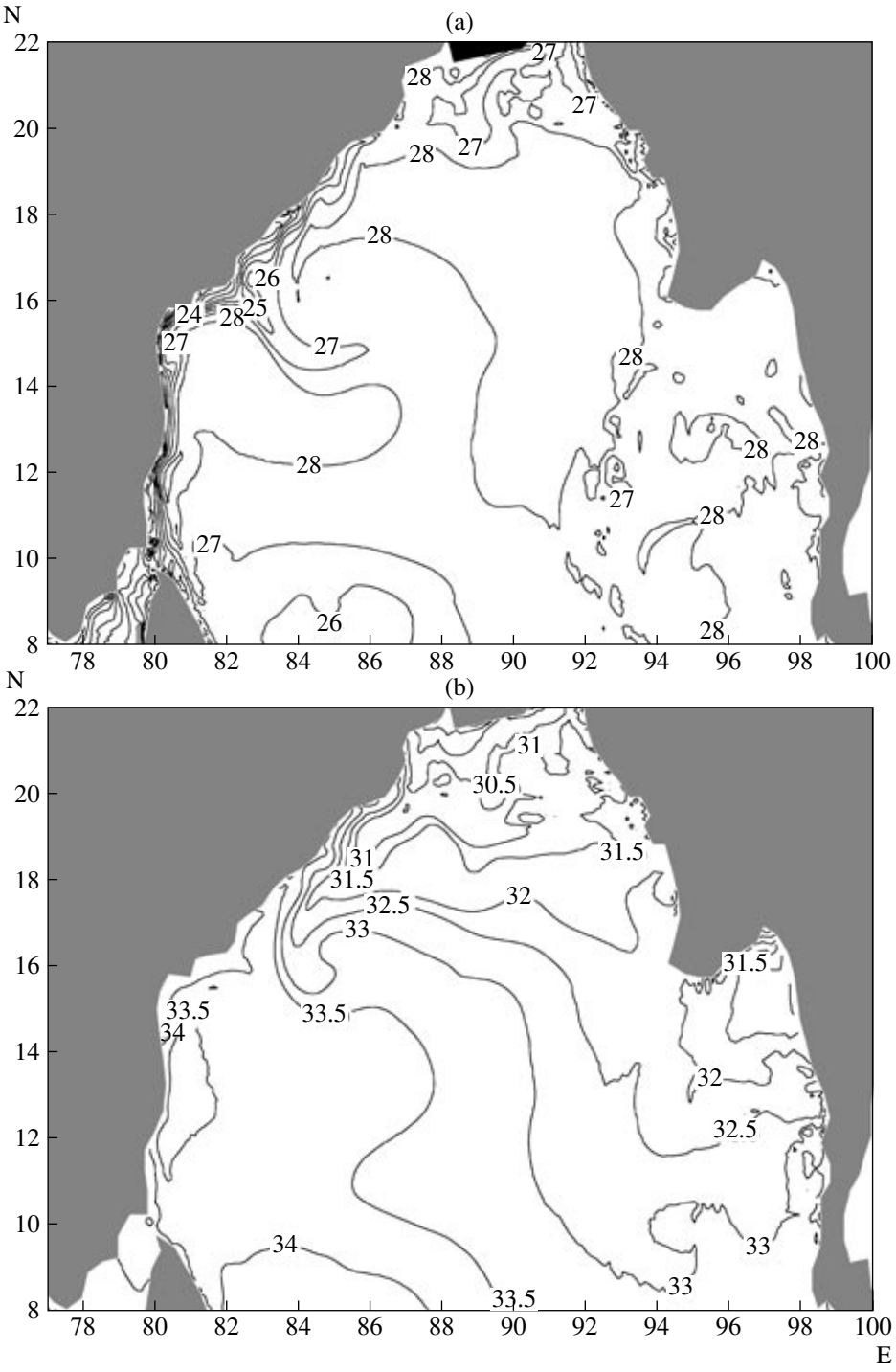

Fig. 8. (a) Temperature (°C) and (b) salinity (‰) in the upper layer of the Bay of Bengal (average values in July).

anticyclone (Fig. 3). In the winter, this anticyclonic gyre disappears (a notable perturbation of the currents near the turn of the coastline continues to exist). A vast anticyclonic rotation of waters appears in the northern half of the bay with velocities on the order of 10 cm/s (Fig. 3a). In January, both peculiarities are distinguished, for example, in the schemes published in [45] and [9].

In order to explain the complex structure of summer currents in the Bay of Bengal, the temperature and salinity fields in July are shown in Fig. 8, which are good markers of the advection process. In the spring and summer, during the intense melting of glaciers in the Himalayas, the Ganges discharges fresh light and turbid waters into the northern part of the bay, which,

due to these properties, is strongly heated by the sun [8]. As a result, a significant salinity decrease and increase in the temperature from the open ocean to the northern part of the bay appear at the surface (Fig. 8). The riverine outflow causes a perturbation in the sea level, which results in an alongshore gradient current of southwestern direction (see Fig. 3b). The propagation of this flow to the south over approximately 750 km is traced well in the fields of salinity and temperature (Fig. 8). A narrow zone of upwelling along the coast caused by the wind forcing is also clearly seen in Fig. 8. This "river-induced" current impacts and mixes with the EICC in the region of 16° N. Under the influence of the wind forcing, it separates from the coast and forms a zone of intense upwelling (Fig. 8a). As a result, a warm pool, which is 1.5–2.0°C warmer than the surrounding basin waters, is formed in the region 13°–15° N near the western coast of India (Fig. 8a). Gradients of level are formed along the periphery of this pool, which generate anticyclonic motion of waters.

Our calculations confirm the scheme of the currents in the Bay of Bengal published in [45] not only for the winter and summer, but also for the entire seasonal cycle (compare Figs. 1, 2). The calculations allow us to state that the principal feature of the formation of the surface current field in the Bay of Bengal is the significant contribution of the gradient currents caused by the riverine outflow (especially in the summer season) to the circulation. In the rest of the Indian Ocean basin north of 10° S, wind forcing is the dominating factor of the current formation.

Currents in the Arabian Sea

The model reproduces well the main large-scale feature of the Arabian Sea dynamics mentioned in all the schemes of the currents mentioned above: monsoon drift currents occupying the entire open part of the Arabian Sea (Figs. 2, 3). In the winter, the Winter Monsoon Current propagates here from the south (Fig. 3a), while in the summer the Summer Monsoon Current originates here (Fig. 3b). In the winter, drift velocities generally do not exceed 20 cm/s (excluding coastal jet currents). In the summer, a region of the maximal summer Monsoon winds absolute for the Indian Ocean develops over the sea, when the mean climatic wind stress in the southwestern part of the sea exceeds 4 d/cm^2; therefore, current velocities in this region reach 100 cm/s or more. In addition to pure drift monsoon currents, the most remarkable feature of the Arabian Sea dynamics is the development of coastal jet currents: the Oman Coastal Current [44] (other names: the East Arabian Current [45] and the West Arabian Sea Current [9]) and the West Indian Coastal Current [44].

The Oman Coastal Current (OCC) is subjected to notable seasonal variations; meanwhile, throughout the entire year, it does not change its northeastern direction along the Arabian Peninsula. It seems that a mistake was made in the scheme [9, Fig. 55] related to the change of its direction in the winter to the southwest according to the forcing by the winter monsoon. In summer, as a result of the upwelling occurring in the OCC near the coast, a significant perturbation of the ocean level is formed. For example, on the basis of satellite data, the authors of [21] showed that, in August, an ocean level decrease in the direction toward the coast appears near the coast of the Arabian Peninsula, which can reach 20 cm or more over 500 km. Then the wind circulation changes to the winter monsoon; however, a weakened flow of the OCC continues its motion to the north. The model reproduced this phenomenon well. In the winter, the velocities in the upper layer of the OCC decrease by almost a factor of two as compared with the summer velocities (Fig. 3); however, a jet flow along the coast continues in the northeastern direction with velocities greater than 20 cm/s. We also note that, in the summer, the jet of the OCC is significantly masked at the surface by the surface drift monsoon flows, which propagate almost normally to the jet (see Fig. 3).

We can state that the general circulation structure in the upper layer of the Arabian Sea is mainly formed due to the wind forcing and features of the coastal boundaries. We note the phenomenon of the West Indian Coastal jet current (WICC); although it is called coastal, it is clearly confined to the shelf break, which is very wide in this region (its width reaches 200–300 km). This current is characterized by reversive monsoon direction changes (Fig. 3). In the summer, the length of the WICC is maximal. It begins in the Gulf of Oman and flows along the coast to the east and south toward the southern end of the Hindustan Peninsula with velocities of 40–70 cm/s (at the surface, drift velocities in certain regions can exceed 100 cm/s). In the winter, the current flows from the Laccadive Islands to the north with velocities of 30–40 cm/s, weakens, and splits into two branches off the northern part of the Kathiavar Peninsula (Fig. 3). The climatic parameters of the WICC calculated by the model are adequate to the summarized field data (see [9, 44, 45] and others).

Quasi-stationary Eddy Formations

Remarkable features of the Indian Ocean dynamics are eddy formations like the Great Whirl and Socotra high [44] near Somali and the Laccadive eddy near the southwestern coast of India, which is manifested as an anticyclonic rotation in the winter (Laccadive high) and a cyclonic rotation in the summer (Laccadive low) (see [44]). An analysis of satellite altimetry data made it possible to record the characteristics of these eddies (see, for example, [21, 30, 44]). These quasi-stationary eddy formations change vorticity sign or even disappear depending on the change of monsoons, but they are stable in their position and have stable spatial sizes. The model adequately reproduced these formations and their parameters and dynamics.

Mean eddy formations based on the mean data for January and July averaged over the layer 20–120 m,

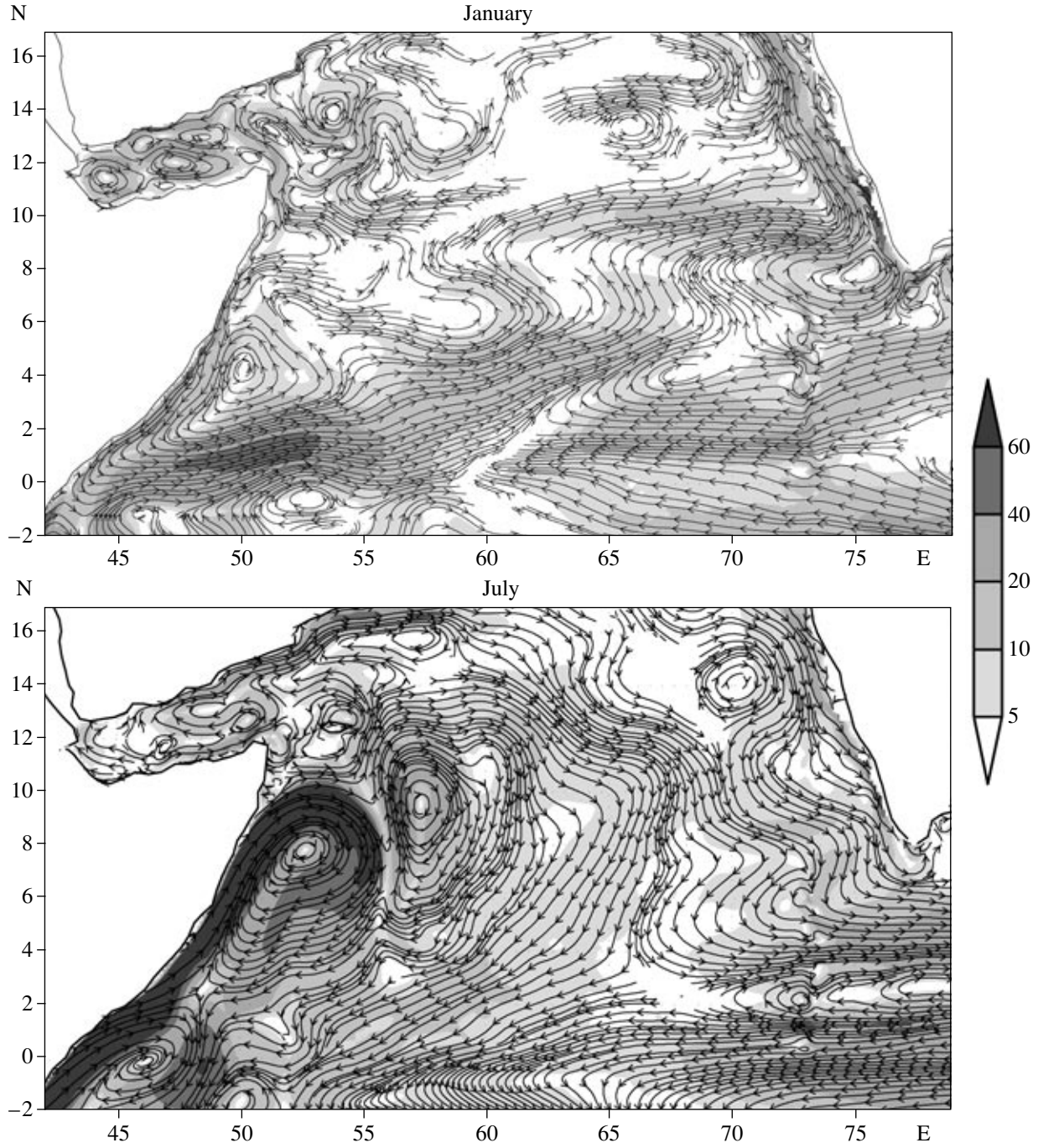

Fig. 9. Streamlines of the velocity of currents averaged over a layer of 20–120 m: (above) mean values for January and (below) mean values for July. Gradations of gray show the velocity values in cm/s (color scale is shown on the right). Velocities below 5 cm/s are not shown.

where they are not masked by drift currents of the upper layers, are shown in Fig. 9. The Great Whirl and the Socotra eddy mentioned above are clearly distinguished. Locations of their centers at 53° E, 8° N, and 57° E, 10° N, respectively, correspond to the data of observations [44]. In the Great Whirl, the velocities reach 2 m/s. The Laccadive gyre is clearly manifested in the results of the modeling, especially in the winter, when its rotation is anticyclonic. Other quasi-stationary eddies are also distinguished. The velocities in these eddies are smaller than the velocities in the principal gyres mentioned above (Fig. 9). The existence of numerous eddy formations is confirmed by the data of satellite altimetry surveys. For example, in August, according to [21], up to 3–4 anticyclones are recorded in the region. This was naturally reflected in the cli-

matic pattern obtained in the experiment using the model with high resolution.

All the eddies mentioned above have a clearly manifested baroclinic character related to the topographic features. The physical causes of their formation require special research beyond the framework of this study.

DISCUSSION AND CONCLUSIONS

Numerical experiments of the circulation in the Indian Ocean were performed using the INM RAS σ model with a high spatial resolution of (1/8)° in longitude and (1/12)° in latitude with 21 nonuniform levels. Annual climatic evolution of the momentum, heat, and freshwater fluxes was specified on the basis of the reanalysis data [26]. Integration was performed over a period of 15 years. Seasonal climatic evolution of current velocities, temperature, and salinity obtained after the 15th calculation year was analyzed and compared with the summarized data of observations [9, 18, 21, 34, 44, 45, and others]. The system of monsoon currents in the upper layer of the ocean and their time evolution and the reversive change in the directions, spatial structure, vorticity, and absolute values of velocities were adequately reproduced. The main components of the monsoon circulation cycle in the Indian Ocean are the Winter Monsoon and the Summer Monsoon currents, which occupy almost the entire basin between Africa and Sumatra north of the equator. The annual monsoon cycle in the southern regions of the Arabian Sea and Bay of Bengal are manifested in the change of the direction of relatively spatially uniform fields of drift monsoon currents. The major part of most intense currents is characterized as jet currents. These are mainly alongshore and near-equatorial currents.

We especially note the adequate simulation of the Somali Current. This is the most powerful western boundary current in the World Ocean, which, unlike the Gulf Stream and Kuroshio, experiences reversive changes its direction following the monsoon regime. Our calculations indicate that the turn of the Somali Current from the northern direction in the summer to the southern direction in the winter is accompanied by the formation of anticyclonic eddies, which propagate to the west as a result of the β effect and later decay either off the Somali coast or in the Gulf of Aden. During the summer monsoon period, the velocities in the Somali Current exceed 2 m/s, and the mass transport exceeds 70 Sv. An analysis of the current velocity field obtained allows us to state that, on the one hand, the SC is formed under the maximal wind stress forcing, and on the other hand it is a compensation jet closing the system of near-equatorial monsoon currents off the coastal barrier. The powerful upwelling in the coastal zone of the Somali Peninsula was simulated. An intense upwelling was also found off the western coast of the Arabian Sea in the jet Oman Coastal Current, which maintains its direction throughout the entire year owing to this effect regardless of the opposite wind monsoon forcing.

The system of near-equatorial currents is a remarkable feature of the Indian Ocean circulation. These currents are formed similarly to the currents in the Atlantic and Pacific oceans by the system of tropical winds, but here their variability is significantly greater. The system of near-equatorial currents varies with a half-year periodicity. The existence of various structural types of jet current combination in the 5–10 degree zone around the equator is observed, such as the Monsoon currents (Winter and Summer), the Equatorial Current, the South Equatorial Current, the Equatorial Countercurrent (between the two latter currents), and the Subsurface Equatorial Countercurrent.

The nature of the Subsurface Equatorial Countercurrent is compensatory with respect to the wind-forced surface current flow at the equator. It is located at depths of 50–400 m in the 2–3 degree neighborhood of the equator. During the periods of its maximal development (velocities up to 40 cm/s), its orientation is always opposite to the surface current at the equator. An increase in the velocity of the SECC to the maximal values occurs with a time lag of approximately one month with respect to the formed surface current of the western or eastern directions at the equator. The monsoon cycle of the SECC is characterized by the phases of eastern (SECCED or Tareev Current) and western (SECCWD) directions. A half-year cycle of circulation near the equator determines two periods of the eastern and western phases. Thus, the SECCED is observed in February–March and October–November, while the SECCWD is observed in June–July and December. During the phase of the eastern direction, the velocities of the SECC on the average are 1.5–2 times greater than those during the phase of the western direction, and the core of the current is located significantly closer to the ocean surface. The total SECCED phase is almost two times longer than the SECCWD phase. Four times a year, when the direction of the surface current at the equator changes, the SECC exists due to inertia and loses its countercurrent property, becoming collinear to the surface current.

The SECCWD is represented by two cores located at 1° north and south of the equator, which is not observed in the eastern phase of the SECC. These differences are explained by the impact of the Coriolis force on the currents of different directions. The vertical (longitudinal structure along the equator) structure of the SECCED is represented by a relatively homogeneous flow, whereas the SECCWD, owing to its deeper location, interacts with the Maldivian Ridge and descends "downstream" west of the ridge by 100–200 m with respect to its part located to the east.

A principal difference was found between the circulation in the northern half of the Bay of Bengal from the circulation in the rest of the Indian Ocean located north of 10° S, where the wind is the dominating factor form-

ing the currents. In the Bay of Bengal, the contribution of the gradient currents that appear due to the riverine outflow becomes the principal factor. This effect is especially strong in the summer season, when the peak outflow of the Ganges River supplies warm turbid fresh waters. This result emphasizes the importance of high-resolution ocean circulation modeling, because, for example, in our paper [7], we did not manage to adequately simulate the currents in the Bay of Bengal with a spatial resolution equal to $1^\circ \times (1/2)^\circ$, although in the rest of the Indian Ocean the general structure of the currents in the upper layer of the ocean was reproduced quite well, taking into account the rough resolution of the model.

The main features of the quasi-stationary eddy structure in the Indian Ocean are reproduced in the model. Large-scale systems such as the Great Whirl, the Socotra high, and the Laccadive high and low known from the data of observations are clearly manifested. Eddies in the convergence zones of jet currents were found (we specially note asymmetric eddies in the convergence zone of the Summer Monsoon and Equatorial currents). The baroclinic gyre near the turn of the coastline of the Hindustan Peninsula in the western part of the Bay of Bengal related to the front of river waters was reproduced in the model. The values of the velocities and spatial sizes of the eddy systems mentioned above are given.

ACKNOWLEDGMENTS

The authors would like to thank Academician of the RAS G.I. Marchuk for his constant attention to the study, discussions, and useful advice. This study was supported by the Federal Agency of the Russian Federation on Science and Innovation within the program "Joint Multidisciplinary Long-Term Program of Scientific and Technical Cooperation between the Agencies of the Russian Federation and Scientific Organizations of the Republic of India," Program no. 17 of Fundamental Research of the Presidium of the Russian Academy of Sciences "Parallel Calculations and Multiprocessor Computational Systems," and by the Russian Foundation for Basic Research (project no. 06-05-64246a).

REFERENCES

1. V. V. Alekseev and V. B. Zalesny, "Numerical Model of the Large-Scale Ocean Dynamics," in *Computing Processes and Systems*, Ed. by G. I. Marchuk (Nauka, Moscow, 1993), No. 10, pp. 232–252 [in Russian].
2. N. A. Diansky, A. V. Bagno, and V. B. Zalesny, "Sigma-Model of the Global Ocean Circulation and Its Sensitivity to the Variations in the Wind Stress," Izv. Akad. Nauk, Fiz. Atmos. Okeana **38** (4), 537–556 (2002).
3. V. F. Kanaev, V. G. Neiman, and N. V. Parin, *Indiiskii okean* (Mysl', Moscow, 1975) [in Russian].
4. V. G. Kort, V. G. Neiman, and V. B. Titov, "Equatorial us of the Indian Ocean during the Winter Monsoon Period," Dokl. Akad. Nauk SSSR **220** (6), 104–108 (1975).
5. G. I. Marchuk, *Methods of Numerical Mathematics*, 2nd ed. (Nauka, Moscow, 1980; Springer, New York, 1975).
6. G. I. Marchuk, V. P. Dymnikov, and V. A. Zalesny, *Mathematical Models in Geophysical Hydrodynamics and Numerical Methods for Their Realization* (Gidrometeoizdat, Leningrad, 1987), 296 p. [in Russian].
7. G. I. Marchuk, V. A. Zalesny, N. A. Diansky, *et al.*, *Modeling the Dynamics of the Indian Ocean and Data Assimilation. Final Report*, Available from IVM RAN, No. 02.200.304060 (Moscow, 1979).
8. S. N. Moshonkin and L. Kharenduprakash, "Influence of Water Salinity and Transparency on the Thermal Properties of the Mixed Layer in the Bay of Bengal," Okeanologiya **31** (3), 384–394 (1991).
9. V. G. Neiman, V. A. Burkov, and A. D. Shcherbinin, "Water Dynamics in the Indian Ocean," Nauchnyi Mir, 232 (1997).
10. *Particular Features of the Thermodynamics and Water Structure in the Tropical Zone of the Indian Ocean*, Ed. by E. I. Lastovetskii and L. I. Stepenko (Gidrometeoizdat, Leningrad, 1982) [in Russian].
11. C. Ramadge, *Meteorology of Monsoons* (Gidrometeoizdat, Leningrad, 1976) [in Russian].
12. A. S. Rusakov and A. N. Diansky, "A Parallel Model of the General Circulation of the Ocean for Multiprocrssor Computing Systems," Informatsionnye Tekhnologii, No. 8, 20–26 (2003).
13. *Oceanology. Physics of the Ocean.* Vol. I. *Hydrophysics of the Ocean*, Ed. by V. M. Kamenkovich and A. S. Monin (Nauka, Moscow, 1978) [in Russian].
14. N. K. Khanaichenko, *System of Equatorial Countercurrents in the Ocean* (Gidrometeoizdat, Leningrad, 1974) [in Russian].
15. A. F. Blumberg and G. L. Mellor, "A Description of a Three-Dimensional Coastal Ocean Circulation Model," in *Three-Dimensional Coastal Models*, Ed. by N. S. Heaps (Amer. Geophys. Union, 1987), Vol. 4, pp. 1–16.
16. K. Bryan, "A Numerical Method for the Study of the Circulation of the World Ocean," J. Comput. Phys. **4**, 347–376 (1969).
17. D. Bryden, S. San, and R. Bleck, "A New Approximation of the Equation of State for Seawater, Suitable for Numerical Ocean Models," J. Geophys. Res. **104** (C1), 1537–1540 (1999).
18. T. P. Boyer and S. Levitus, *Objective Analysis of Temperature and Salinity for the World Ocean on a 1/4 Degree Grid* (NOAA Atlas NESDIS 11, 1997).
19. O. Boebel, C. Barron, P. Richardson, et al., "Mixing of Antarctic Intermediate Water from the Atlantic and Indian Oceans at the Aghulhas Retroflection," International WOCE Newsletter, No. 39, 9–12 (2000).
20. M. D. Cox, *A Primitive Equation Three-Dimensional Model of the Ocean. GFDL Ocean Group Technical Report No. 1. Available from Geophysical Fluid Dynamical Laboratory*, No. 08542 (Princeton, New Jersey, 1984).
21. J. Fischer, F. Schott, and L. Stramma, "Currents and Transports of the Great Whirl–Socotra Gyre System dur-

ing the Summer Monsoon, August 1993," J. Geophys. Res. **101**, 3573–3588 (1996).

22. U. Garternicht and F. Schott, "Heat Fluxes of the Indian Ocean from a Global Eddy-Resolving Model," J. Geophys. Res. **102** (C9), 21147–21159 (1997).
23. S. M. Griffies, C. Boning, F. O. Bryan, et al., "Developments in Ocean Climate Modelling," Ocean Model. **2**, 123–192 (2000).
24. S. Hellerman and M. Rosenstein, "Normal Monthly Wind Stress over the World Ocean with Error Estimates," J. Phys. Oceanogr. **13**, 1093–1104 (1983).
25. N. Jerlov, *Optical oceanography* (Elsevier, 1968).
26. E. Kalnay, M. Kanamitsu, R. Kistler, et al., "The NCEP/NCAR 40-Year Reanalysis Project," Bull. American Meteorological Society **77**, 437–471 (1996).
27. M. R. Kumar and S. S. C. Shenoi, "On the Role of the Cross Equatorial Flow on Summer Monsoon Rainfall over India Using NCEP/NCAR Reanalysis Data," Meteorology and Atmospheric Physics **70**, 201–213 (1999).
28. T. Lee, I. Fukumori, D. Menemenlis, et al., "Effects of the Indonesian Throughflow on the Pacific and Indian Oceans," J. Phys. Oceanogr. **32** (5), 1404–1429 (2002).
29. S. Levitus, *World Ocean Atlas*, CD-ROM Data Set (U.S.Department of Commerce, National Oceanic and Atmospheric Administration, National Environmental Satellite Data and Information Service, National Oceanographic Data Center, Ocean Climate Laboratory, 1994).
30. J. W. Lopez and L. M. Kantha, "A Data-Assimilative Numerical Model of the Northern Indian Ocean," J. Atm. Oceanic Technology **17**, 1525–1540 (1999).
31. G. I. Marchuk, A. S. Rusakov, V. B. Zalesny, and N. A. Diansky, "Splitting Numerical Technique with Application to the High Resolution Simulation of the Indian Ocean Circulation," Pure Appl. Geophys., 1407–1429 (2005).
32. J. P. McCreary and P. K. Kundu, "A Numerical Investigation of the Somali Current during the Southwest Monsoon," J. Marine Res. **46** (1), 25–58 (1988).
33. J. P. McCreary, P. K. Kundu, and R. L. Molinari, "A Numerical Investigation of Dynamics, Thermodinamics, and Mixed Layer Processes in the Indian Ocean," Progr. Oceanogr. **31** (1993).
34. M. J. McPhaden, "Variability in the Central Equatorial Indian Ocean: Part I. Ocean Dynamics," J. Marine Res. **40**, 157–176 (1982).
35. F. Mesinger and A. Arakava, "Numerical Methods Used in Atmospheric Models," Global Atmos. Res. Prog. (GARP) WMO–ICSU Joint Org. Committee **1** (17), (1976); Gidrometeoizdat, Leningrad, 1979.
36. R. C. Pacanovsky and G. Philander, "Parametrization of Vertical Mixing in Numerical Models of the Tropical Ocean," J. Phys. Oceanogr. **11**, 1442–1451 (1981).
37. R. C. Pacanovsky and S. M. Griffies, *The MOM 3 Manual* (Geophysical Fluid Dynamics Laboratory, NOAA, Princeton, USA, 1999).
38. T. G. Prasad and M. Ikeda, "The Wintertime Water Mass Formation in the Northern Arabian Sea," J. Phys. Oceanogr. **32** (3), 1028–1040 (2002).
39. C. S. Ranage, F. R. Miller, and C. Jeffries, *Meteorological Atlas of the International Indian Ocean Expedition* (N.S.F., 1972), No. 1.
40. A. Schiller, J. S. Godfrey, P. C. McIntosh, et al., "Seasonal Near-Surface Dynamics and Thermodynamics of the Indian Ocean and Indonesian Throughflow in a Global Ocean General Circulation Model," J. Phys. Oceanogr. **28** (11), 2288–2312 (1998).
41. F. Schott, J. C. Swallow, and M. Fieux, "The Somali Current at the Equator: Annual Cycle of Current and Transports in the Upper 100 m and Connection to Neighbouring Latitudes," Deep-Sea Res. **37**, 1825–1848 (1990).
42. F. Schott and J. P. McCraeary, "The Monsoon Circulation of the Indian Ocean," Progr. Oceanogr. **51**, 1–123 (2001).
43. A. J. Semtner, *A General Circulation Model for the World Ocean with Bottom Topography*, (UCLA Dept. of Meteo. Techn. Rep. No. 8, 1974).
44. D. Shankar, P. N. Vinayachandran, A. S. Unnikrishnan, and S. R. Shetye, "The Monsoon Currents in the North Indian Ocean," Progr. Oceanogr., No. (1), 63–119 (2002).
45. M. Tomczak and J. S. Godfrey, *Regional Oceanography* (Butler and Tanner Ltd., Great Britain, 2003).
46. Y. You, "Seasonal Variations of the Thermohaline Circulation and Ventilation in the Indian Ocean," J. Geophys. Res. **102** (C5), 422 (1997).